Improvement of atmospheric ammonia emissions combined with satellite observations

Miaomiao Cheng[1]*, Jun-ichi Kurokawa[2], and Keiichi Sato[2]

[1]* Institute of Atmospheric Environment, Chinese Research Academy of Environmental Sciences, Beijing 100012, China

[2] Asia Center for Air Pollution Research, 1182 Sowa, Niigata, 950-2144, Japan.

Abstract

The increasing of atmospheric nitrogen deposition has been becoming significant due to amount of nitrogen emissions caused by human activities in regional and global areas. At present, China has become another high nitrogen deposition region besides North America and Europe. However, a major challenge in developing effective nitrogen emission control measures is necessity of accurate assess of atmospheric nitrogen emissions in these regions. In response to this scientific problem, this project uses the mainland of China as a study area to address the lack of accuracy of atmospheric nitrogen emission inventories (EIs) and construct inventory inversion models to improve the accuracy of bottom-up emission inventories using time-series remote sensing data. Firstly, the ground-based NH_3 concentrations were used to assess the applicability of the long-series IASI NH_3 column over the whole country. The results showed that the spatial and temporal variations of IASI NH_3 column concentrations are consistent with those of the ground-observed NH_3 concentrations in the study area. The NH_3 EI was improved using atmospheric chemical transport models and satellite observation data based on the inverse modeling (IM) approach. The near-ground observation data were used to validate the accuracy of improved NH_3 EI. In this study, for improvement of NH_3 EI, corrections of acidic gas emissions as well as those of monthly profile of NH_3 emissions were conducted because concentration of gaseous NH_3 in the atmosphere is affected not only by its emissions, but also by concentrations of acidic gases. In order to accurately assess the uncertainties in bottom-up NH_3 emissions in China, this study first corrects for the acidic gas (SO_2) emissions before adjusting the NH_3 emission inventory using IM combined with the near-ground SO_2 observations. The simulated SO_2 results using the improved SO_2 emissions are in good spatial and temporal agreement with observations. After that, the monthly NH_3 emission profile was improved based on satellite observations, and the validation results based on near-ground NH_3 observation data showed that the reliability of the improved NH_3 emission inventory in terms of spatial distribution and temporal trends. Analysis of improved NH_3 emissions shows that NH_3 emissions are mainly concentrated in densely populated areas such as the North China Plain, Yangtze River Delta, Pearl River Delta, and Chengdu-Chongqing region, with emissions greater than 300 kg ha^{-1} yr^{-1}; in terms of recent trends, China's NH_3 emissions have basically stabilized at around 10 million tons/year from 2013 to 2016. The results of this study provide a scientific and effective reference basis and technical methods for improving regional research on

atmospheric nitrogen emissions and the outcomes of this project will strengthen the utilization of satellite data on regional atmospheric nitrogen cycle.

Keywords: Ground-based observations, Spaceborne remote sensing, IASI NH$_3$ columns， emission inventories, inverse modeling

1. Introduction

In recent decades the nitrogen gas emissions significantly increased in the atmosphere mainly due to the burning of fossil fuels, the production and use of nitrogen fertilizer, plenty of livestock breeding and other human activities. The emissions, transport, chemical conversion and the subsidence process of the reactive nitrogen has migrated and redistributed in the regional and global scale. It has become a research hotspot in the field of nitrogen cycle (Galloway et al., 2008, Lu and Tian 2007, Liu et al., 2013, Zhao et al., 2015). With the intensification of human activities, the annual global nitrogen gas emissions into the atmosphere have increased from 9.9 Tg N yr^{-1} in 1860 to 74 Tg N yr^{-1} in 2010 (Fowler et al., 2013; Galloway et al., 2002), among which the total global ammonia emissions were as high as 59.3 Tg N yr^{-1} in 2020 (Sutton et al., 2013). China's total NH$_3$ emissions increased from 4.9 Tg N yr^{-1} in 1980 (Kang et al., 2016) to 17.2 Tg N yr^{-1} in 2010 (Gu et al., 2013), nearly three times higher than the combined annual emissions of the European Union and the United States (6.3 Tg N yr^{-1}) (Gu et al., 2013). Numerous studies have shown that the annual global deposition of reactive nitrogen into various ecosystems is as high as 43.5×10^6 t (Galloway and Cowling 2002, Holland et al., 1999). High nitrogen deposition not only interferes with or changes the cycling process of the regional ecosystem (Magill et al., 2000, Mo et al., 2004), but also damages the balance of the natural environment system, resulting in a series of ecological environment deterioration from the regional to the global scale (Liang et al., 2014, Liu et al., 2006). In order to relieve environmental pressure and solve the problem of high nitrogen deposition caused by human activities, accurate estimation of nitrogen gases emissions is the prerequisite and necessary basis for effective nitrogen emission reduction control measures.

There is a larger uncertainty for Chinese air pollutants emission inventories in regional and national scale, due to the incomplete coverage and complex composition of pollution sources, the rapid updating of pollution control techniques and unavailability data. The atmospheric pollutant column concentration data based on satellite remote sensing monitoring has the characteristics of wide space coverage, strong time continuity and convenient data acquisition, so as to provide a real-time and reliable reference for the improvement and update of emission inventory. Exploratory studies have been carried out to improve the accuracy of emission inventory by using satellite data (Streets et al., 2013). A number of researchers used NO$_2$ data from satellite observations to retrieve NOx emission inventories in the world (Martin et al., 2006), Europe (Zyrichidou et al., 2014) and Asia (Kurokawa et al., 2009; Zhao and Wang 2009) and achieved good results. In China, Zhang et al. (2007) calculated the NOx emission trend from 1995 to 2004 and evaluated them using NO$_2$ observed by satellite. Lin et al. (2012) used NO$_2$ data from satellite observations to invert NOx emissions from human activities, lightning and soil in eastern China in 2006. The preliminary results show that the top-down source emission inventory inversion model based on satellite observation data can well reduce the

uncertainty in the inventory and improve the accuracy and reliability of the simulation results of atmospheric nitrogen deposition. This study uses satellite remote sensing data and inversion model to improve the accuracy of NH_3 emission inventory in order to provide data support for regional atmospheric nitrogen emission management.

2. Data and Methodology

2.1 The procedures for improvement of emissions

The schematic diagram of this study as shown in Figure 1-1. As discussion above, the concentration of gaseous NH_3 in the atmosphere is affected not only by its emissions, but also by concentrations of acidic gases. Therefore, there were two steps for improving NH_3 emissions. Firstly, SO_2 emission was adjusted based on the near-ground observations using inverse model. Then spatial pattern and monthly profile of NH_3 were adjusted based on satellite data. The collected near-ground NH_3 concentrations was used to validate the simulated concentrations based on the improved emission inventory (E").
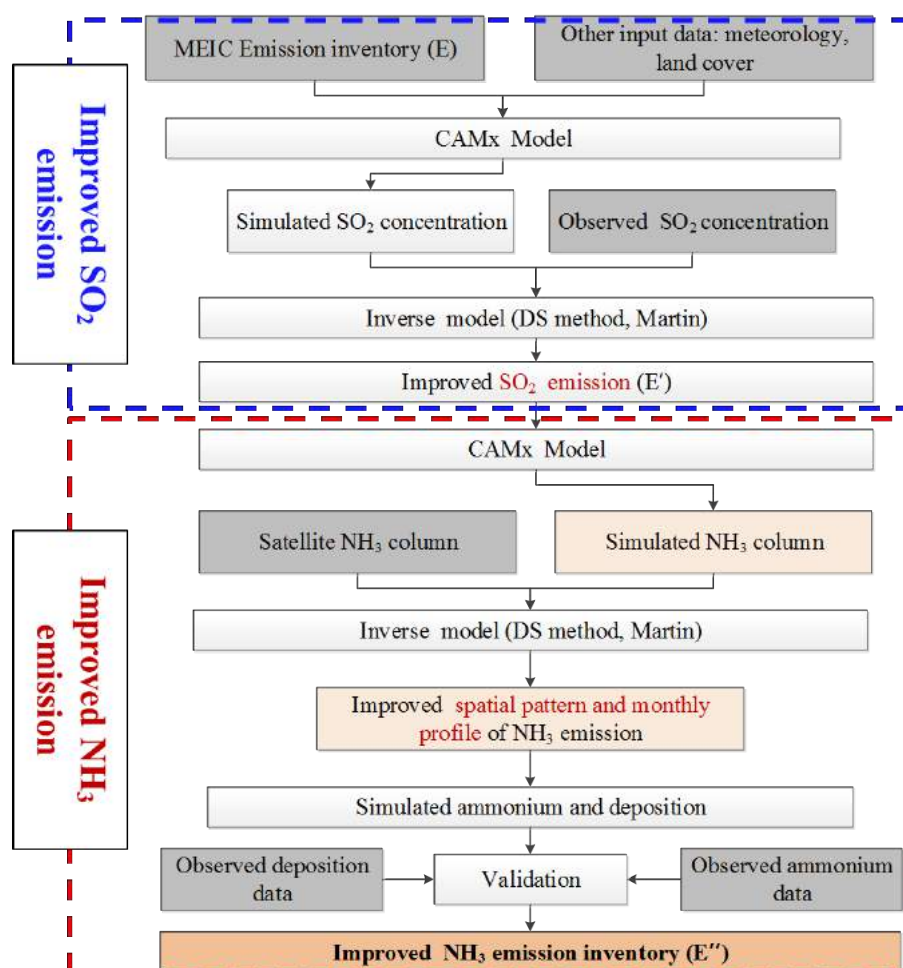

Figure 1-1. Schematic diagram of this study.

2.2 Study area

In this study, inversion of nitrogen emissions and deposition were carried out in mainland China. Considering that the monitoring of major air pollutants in China began to be routinely

monitored in 2013, in order to better verify the simulation results of the model with ground monitoring data, the simulation period of this study was selected from January 2013 to December 2016, for a total of 48 months (4 years). China's land use types and population distribution in 2010 are shown in Figure 2-1. The altitude of China has been descending from west to east. The mountainous area of China accounts for 2/3 of the total area of the country and has advantages in the development of forestry, stock farming, tourism and mining. The plain area only accounts for 1/3 of the total area of China. The Northeast Plain, the North China Plain and the Middle-Lower Yangtze plains are the three great plains in China. They are all distributed in the east of China. From the perspective of population distribution, China's population is concentrated in the east of the "Heihe-Tengchong" line proposed by Hu Huanyong (She W, 1998), presenting a multi-center of spatial and agminated pattern. The population density is generally above 500 people /km^2, among which the Yangtze River Delta, Pearl River Delta, Beijing-Tianjin-Hebei and Chengdu-Chongqing regions are highly densely populated areas over than 1000 people /km^2.
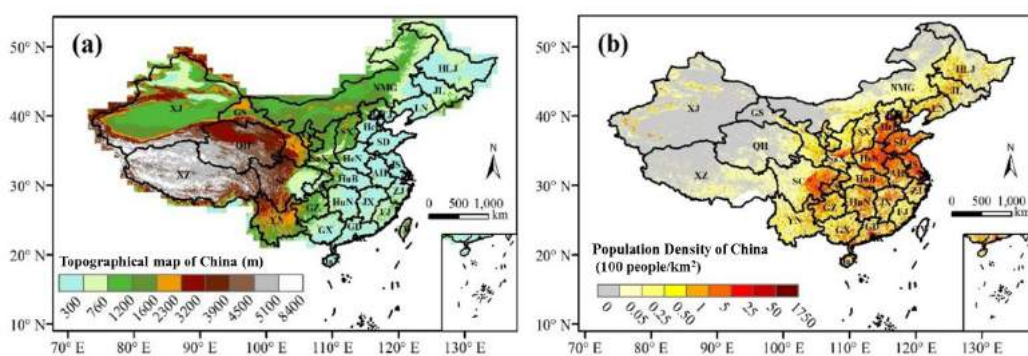

Figure 2-1. Topographic of China (a) and population distribution of 2010 (b).

2.3 Emission inventory

The initial NH$_3$ emission inventory from 2008 to 2016 is derived from the MEIC inventory produced by Tsinghua University. MEIC is built based on INTEX -B data set and updated based on the Technical guidelines for the compilation of emission inventories of air pollutant sources released by Ministry of ecology and environment of China (MEE) (MEE, 2015), with involving energy, industrial, residential, agriculture, road and off-road vehicles, biomass combustion sources, etc. The air pollutants of MEIC include SO$_2$, NOx, CO, NMVOC, PM$_{10}$, PM$_{2.5}$, BC, OC, NH$_3$, etc (Liu et al., 2015). MEIC is considered to be the first air pollutants emission inventory in China based on a consistent methodology and widely used in national air quality improvement management (Liu et al., 2015; Cheng et al., 2017; Zheng et al, 2017). NH$_3$ emission inventory is developed by Peking University and constantly updated to improve the spatio-temporal resolution, which has been verified through a number of studies (Huang et al., 2012; Kang et al., 2016; Li et al., 2017). MEIC is updated every two years and provides gridded emission data with a spatial resolution of 0.25°×0.25°.

The simulation period of this study is from 2013 to 2016, and the region is in mainland China. The original data of source emission inventory is based on 2012-2016 MEIC emission inventory, and emissions in 2008 of REAS 2.1 (Kurokawa et al., 2013) was used as foreign source inventory data. The input emission inventory file for CAMx model was integrated into model grid after time profile, species allocation and grid processing. The main sources include

industry, traffic, residential sources, agriculture, power plant sources, etc. Figure 2-2 shows the distribution of annual emissions per unit area of NH_3 (unit: kg N ha^{-1} yr^{-1}). It can be seen that NH_3 emissions are concentrated in densely populated areas such as the North China Plain, Yangtze River Delta, Pearl River Delta and Sichuan Basin, and emit more than 40 kg N ha^{-1} yr^{-1}.
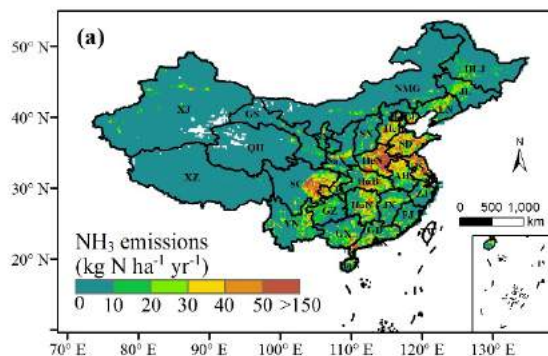

Figure 2-2. Spatial distribution of NH_3 emissions based on MEIC inventory of China in 2014.

2.4 Tropospheric NH_3 column observed by satellite

The NH_3 satellite observations used in this study were obtained from a new generation of ultra-high spectral Atmospheric detector — Infrared Atmospheric Detector Interferometer (IASI), which is one of the key instrument aboard MeTOP-A launched in October 2006. MeTOP-A passes from north to south over the equator at 09:30 per day and measures the infrared radiation emitted by the earth's surface and atmosphere (Clarisse et al., 2009). The detection wavelength range of the IASI is 362 nm-1550 nm, the spectral resolution is 8-70nm, and the spatial resolution in nadir is 12 km and increases to 39 km and 20 km for edges (Van Damme et al., 2015). The temporal resolution is twice a day, and the transit time is usually 09:30 and 21:30 in local time. IASI-NH_3 product is based on the calculation of hyperspectral range index, which is converted into NH_3 column through neural network algorithm and the detailed method can be seen in Whitburn et al. (2016). Some studies have found that the thermal contrast is higher in the morning of a day, and the satellite is more sensitive to NH_3 at the morning transit (Van Damme et al., 2017; Liu et al., 2017a, b). In this study, we will further verify the applicability of tropospheric IASI-NH_3 columns in China. The satellite-based NH_3 column concentration data product is the daily mean value of L2 data obtained from the Website IASI (https://iasi.aeris-data.fr/NH3/), with a spatial resolution of 0.25°×0.25°. The data period used in this paper is 1 January 2008 to December 31, 2016. Only the observation results with a cloud coverage of less than 25% and an absolute error of less than $5×10^{15}$ mole cm^{-2} were selected. In data processing, the daily average of observation points in each grid cell is used to calculate the monthly arithmetic average. Similarly, we calculate the annual mean by averaging the daily mean of the observation points in the grid cell throughout the year.

2.5 Near-ground verification data set

The data from Chinese Nationwide Nitrogen Deposition Monitoring Network (NNDMN) (provided by Agricultural University of China) were used to assess the applicability of IASI satellite NH_3 column on different land covers in China. NNDMN monitoring is in line with international standards, and monitoring sites are as far away from local direct emission sources

as possible to improve regional representation. According to their geographical location and proximity to major emission sources, they can be divided into three categories: urban stations, rural stations and background stations. A detailed description of all sites, including the surrounding environment and nearby emission sources, can be found in Xu et al. (2015, 2018). In this study, the monthly mean of NH_3 concentration over different land covers of 25 stations from 2010 to 2015 was used (Table 2-1), and its spatial distribution is shown in Figure 2-3.

Table 2-1. Station information of NH_3 concentration observation.

| Land cover types	Sites	Lon	Lat	Period
Urban regions	CAU	116.28°E	40.02°N	Apr.2010-Dec.2015
	ZZ	113.63°E	34.75°N	May.2010-Dec.2015
	DL	121.58°E	38.92°N	Sep.2010-Dec.2015
	NJ	118.85°E	31.84°N	Jan.2011-Dec.2011, Jan.2015-Dec.2015
	BY	113.27°E	23.16°N	May.2010-Dec.2015
	WJ	103.84°E	30.55°N	Oct.2010-Dec.2015
Rural regions	SZ	116.20°E	40.11°N	Apr.2010-Dec.2015
	QZ	114.94°E	36.78°N	Apr.2010-Dec.2015
	YQ	112.89°E	38.05°N	Apr.2010-Dec.2015
	YL	108.01°E	34.31°N	Apr.2010-Dec.2015
	YC	116.63°E	36.94°N	Sep.2012-Dec.2015
	GZL	124.83°E	43.53°N	Jul.2010-Dec.2015
	LS	124.17°E	43.36°N	Jul.2010-Dec.2015
	WX	115.79°E	30.01°N	Aug.2011-Dec.2015
	TJ	111.97°E	28.61°N	Oct.2010-Dec.2015
	ZZ	110.33°E	21.26°N	Aug.2010-Dec.2015
	FZ	119.36°E	26.17°N	Apr.2010-Dec.2015
	FH	121.53°E	29.61°N	Aug.2010-Dec.2015
	ZY	104.63°E	30.13°N	Jul.2010-Dec.2015
	YT	105.47°E	31.28°N	May.2011-Dec.2013
	JJ	106.18°E	29.06°N	Jan.2013-Dec.2015
Background	HN	113.41°E	28.52°N	Sep.2010-Dec.2015
	XS	113.31°E	28.61°N	Sep.2010-Dec.2015
	LSD	120.18°E	35.77°N	Feb.2011-Dec.2015
	CD	120.75°E	37.93°N	Sep.2010-Dec.2015
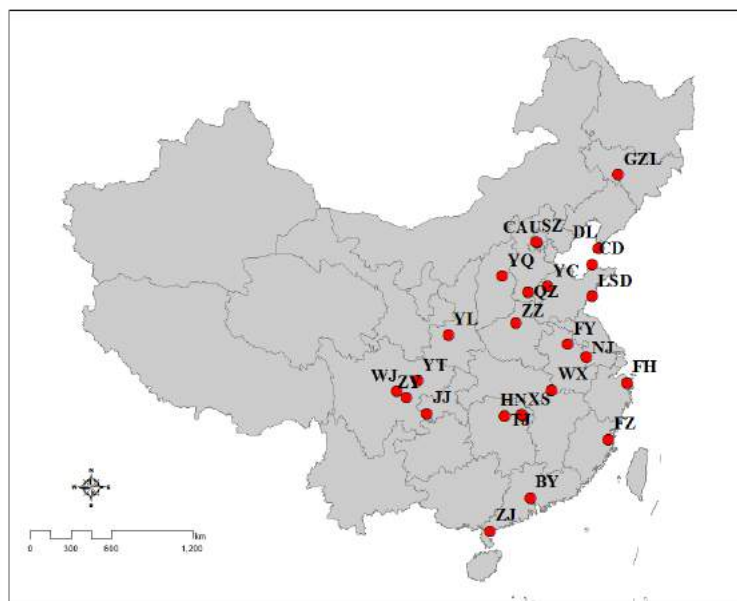
Figure 2-3. Spatial distribution of NNDMN network stations.

2.6 Description of Chemical Transport Model

We employed the WRF-CAMx model for simulating the effects of NH_3 emission improvement. CAMx is the third generation of three-dimensional model for air quality developed by ENVIRON company in the United States. It can simulate the emission, transport, chemical reaction and removal of pollutants in the troposphere, and apply to the comprehensive simulation study of photochemical smog and fine particulate air pollution at multiple scales. The meteorological data is provided by the Weather Research and Forecasting (WRF) model. In this study, the areas of simulation covered the whole China, Northeast Asia and parts of Southeast Asia with a horizontal grid resolution is 36 km × 36 km. The model is setup with 20 terrain-following hydrostatic vertical pressure (σ) coordinates.

2.7 Method of inversion model

Inversion model algorithm includes linear and nonlinear. Nonlinear algorithm including Kalman filter and the four-dimensional variational assimilation, the advantage of these two methods are to consider the chemical conversion process and the sensitivity analysis for different emission source contribution rate. Therefore, these two methods involve more variables and large amount of calculation and are generally used in a short time, small scale regional emissions improvement. The linear algorithm mainly refers to the method used by Martin et al. (2003, 2008) in the inversion of NO_2 emission inventory. Based on the principle of substance conservation, the inversion of pollutant emissions involves fewer parameters and requires less calculation. In this paper, a linear algorithm was selected to correct and improve of MEIC NH_3 emissions. The equation is shown as following:

$$E^{'} = E_b \times \frac{\Omega_s}{\Omega_m} \quad \dots\dots\dots\dots\dots\dots\dots\dots\dots\dots\dots\dots\dots\dots(2.1)$$

Thus, E' is the improved NH_3 emissions, Ω_s is the IASI NH_3 columns, Ω_m is the simulated NH_3 columns，E_b is the initial emissions.

The method is developed based on a global model with a coarse resolution grid and assumes that the pollutants concentration in the air for each model grid is not affected by the

emissions from the surrounding grid. However, in the regional model with relatively fine resolution grid, this assumption may not be true. When the lifetime of pollutants in the atmosphere is longer than the horizontal transmission time, there will be spatial dispersion error (Martin et al., 2003; Boersma et al., 2008; Lamsal et al., 2010; Turner et al., 2012).

3. Verification of IASI NH₃

Although the product of IASI NH₃ have been compared with the near-ground NH₃ concentration by some researchers in different spatial and temporal scale, considering that NH₃ column observed by satellite is the key data source of inverse model in this study, this part further evaluates the applicability and reliability of the newest IASI NH₃ products in a long time and nationwide scale using relatively accurate ground observation NH₃ concentration.

3.1 NH₃ satellite product selection

Now there are two products of IASI NH₃ with different algorithm: one is the NH₃ column retrieved in real time, labeled as IASI_NH₃_v1; the other is retrieved in real time, which can be further corrected based on reanalysis of temperature and relative temperature profile to obtain a more accurate NH₃ column product, labeled as IASI_NH₃_R. The spatial distribution of this two products are shown in Figure 3-1. They are basically the same, but the value of IASI_NH₃_R column is higher than IASI_NH₃_v1 in east of China.
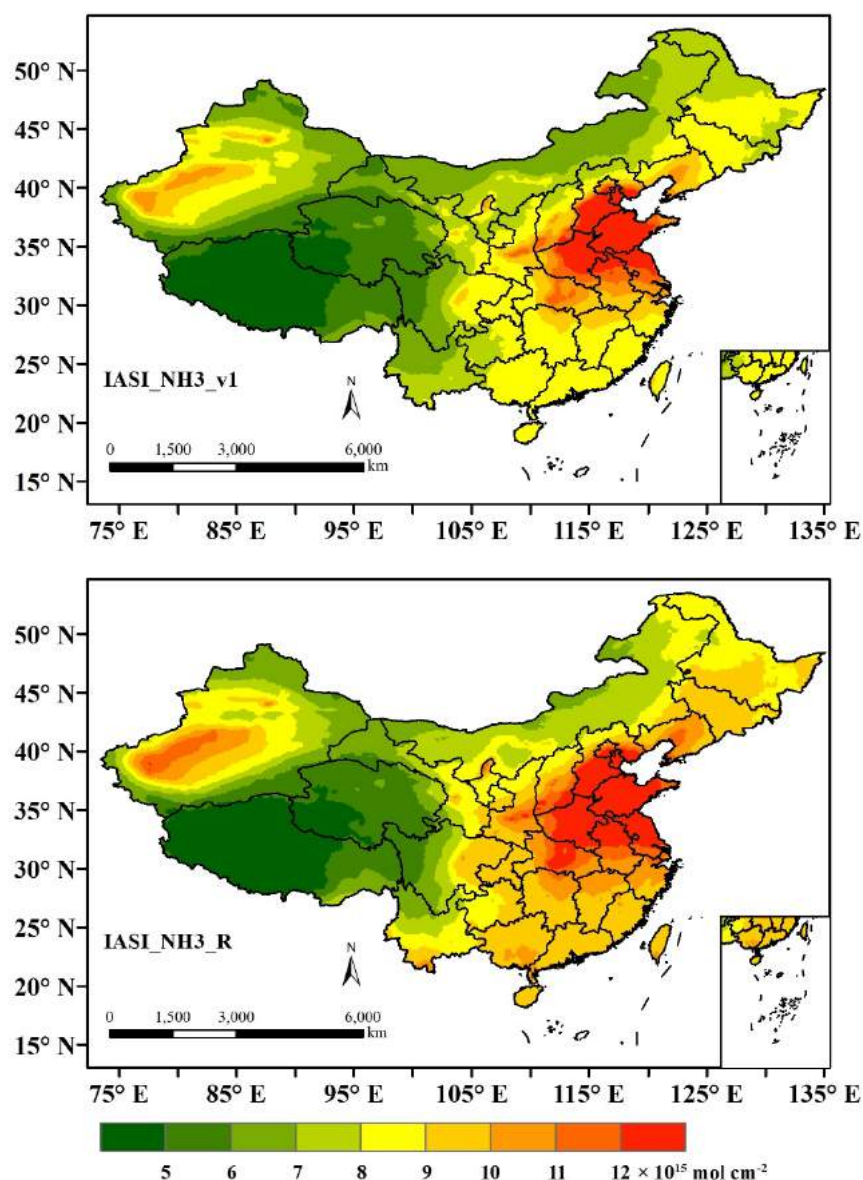
Figure 3-1. Comparison between IASI-NH$_3$-v1 (top) and IASI_NH$_3$_R (down) NH$_3$ products in China.

The correlation between IASI_NH$_3$_R and IASI_NH$_3$_v1 products is shown in Figure 3-2. The overall correlation between them is good, with a correlation coefficient of 0.93. From the distribution of values, IASI_NH$_3$_R product was significantly higher than IASI_NH$_3$_v1 when it was over 12×10^{15} mole cm^{-2}, and lower than IASI_NH$_3$_v1 product while less than 12×10^{15} mole cm^{-2}. It can be seen that IASI_NH$_3$_R product has a wide range of concentration values, which can better reflect the spatio-temporal heterogeneity of atmospheric NH$_3$.
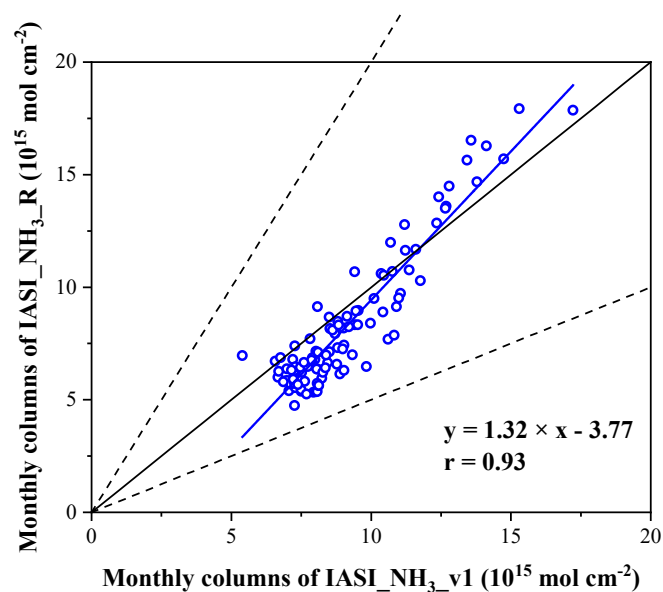
Figure 3-2. Scatter plot of monthly NH₃ columns between IASI-NH₃-v1 and IASI_NH₃_R in China.

3.2 Validation of IASI NH₃

As above result, IASI_NH₃_R was selected in this study to analyze the distribution characteristics of NH₃ in the atmosphere in China. In order to assess the accuracy of IASI_NH₃_R products, the monthly mean IASI NH₃ columns were compared by the near-ground monthly mean NH₃ concentrations on 25 NNDMN sites in eastern China.

Figure 3-3 shows the comparison of the annual mean value (Figure 3-3 a) and growth rate (Figure 3-3 b) between IASI NH₃ column and NNDMN NH₃ concentration. Figure 3-3 c, d show the corresponding scatter distribution, linear regression fitting and correlation coefficient. From 2010 to 2015, the annual average NH₃ concentration and its growth rate (Figure 3-3 a, b) in satellite and near-ground observations show similar spatial patterns, and the higher values appears in North China. There was a significant positive correlation between IASI NH₃ column and NNDMN NH₃ concentration ($r=0.71$, $p<0.001$, Figure 3-3 c). These results indicate that the accuracy of IASI NH₃ reanalysis product is consistent with that of IASI NH₃ product in near real-time (Van Damme et al., 2015; Xu et al., 2018), but the former is more suitable for evaluating interannual changes and trends (Van Damme et al., 2017). In addition, the annual growth rate between satellite and ground observations was significantly positive ($r=0.81$, $p<0.001$, Figure 3-3 d). The above results indicate that IASI NH₃ can better reflect the spatial pattern and annual variation trend of atmospheric NH₃ in China.

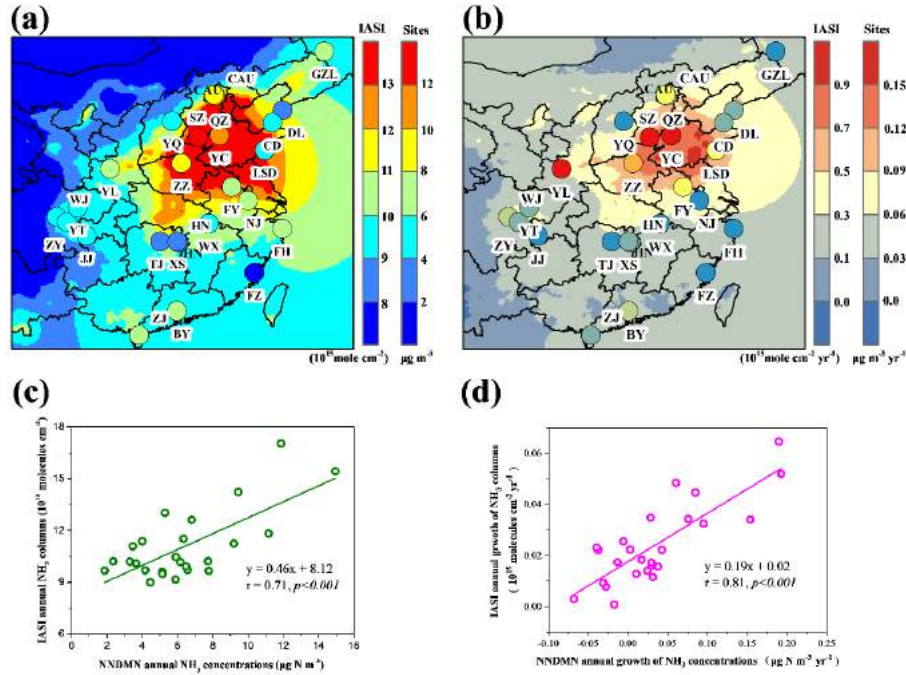Figure 3-3. Spatial variation of atmospheric NH₃ in eastern China: (a) annual means of NNDMN NH₃ concentrations vs. IASI_NH₃_R columns; (b) annual growth rates of NNDMN NH₃ concentrations vs. reanalyzed IASI_NH₃_R columns; (c) relationship between annual means of NNDMN_NH₃ concentrations vs. IASI_NH₃_R columns; (d) relationship between annual growth rates of NNDMN_NH₃ concentrations vs. IASI_NH₃_R columns.

4. Results and discussions

4.1 Comparison of tropospheric NH₃ column based on initial EI with satellite observations

The temporal comparison between simulated troposphere NH₃ columns based on MEIC in China during 2013-2016 and IASI NH₃ observations columns is shown in Figure 4-1. Simulated NH₃ columns are obviously lower than IASI NH₃ columns. the monthly differences between them ranged from $-18 - -2 \times 10^{15}$ mole cm⁻² and have significant seasonal trend with higher in summer and lower in winter.
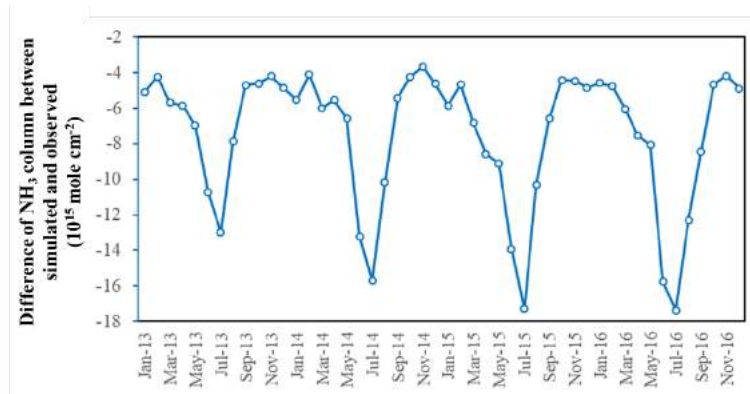

Figure 4-1. Difference of monthly NH₃ column between MEIC simulation and IASI observation.

The spatial comparison between simulated tropospheric NH_3 columns based on MEIC in China during 2013-2016 and IASI NH_3 observations columns is shown in Figure 4-2. Simulated tropospheric NH_3 column over China are lower than IASI NH_3 observations, spatially in Beijing-Tianjin-Hebei and its surrounding region (BTHs), Yangtze River Delta (YRD), Fenhe-Weihe Basin (FWB), Northeast China (NEC), South China (SC) and Xinjiang oasis agriculture area (XJO). According to the physical and chemical processes of NH_3 in the atmosphere, there are two possible reasons for the underestimation of simulated NH_3 column. One is that the underestimation of NH_3 emissions, and the other is that the overestimation of acidic gases emission in the atmosphere which leads to the underestimation of NH_3 column concentration.
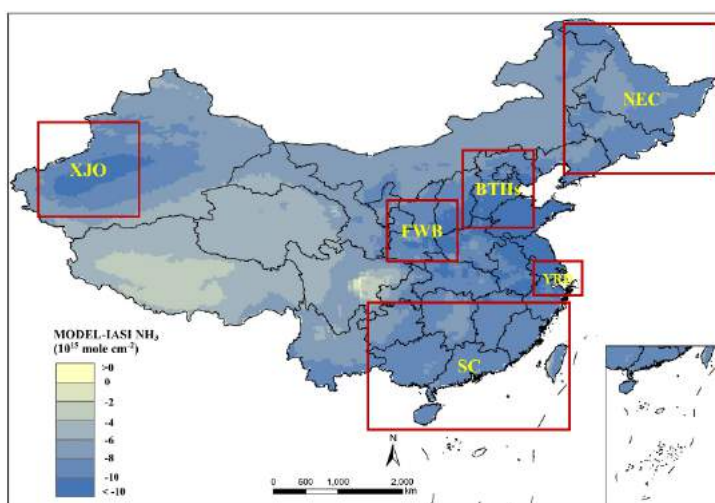

Figure 4-2. Differences of NH_3 column between MEIC simulation and IASI observation.

4.2 Improvement of NH_3 emissions

As discussed in section 4.1.1, there is great uncertainty in the quantitative analysis of NH_3 column between simulated results based on MEIC and IASI observation. The results of several NH_3 emission inventories (Huang et al., 2012; Kang et al., 2016; Liu et al., 2017a, 2017b, 2019) show that amount of China's NH_3 emission is about 10 million tons/year. While the total emission of NH_3 in MEIC is consistent with the other research results, it is possible that the low simulated NH_3 column may be caused by the overestimated emission of acid gas (such as SO_2). Therefore, the method of improving NH_3 emission is mainly divided into two steps: firstly, the SO_2 emissions as a key acid gas in the air was adjusted based on near-ground observation; then, spatial and monthly profile of NH_3 emission will be improved based on the variation of monthly IASI NH_3 columns.

According to the process of atmospheric chemistry, NH_3 is the key alkaline gas in the atmosphere, and its emissions mainly come from agriculture such as fertilizer and livestock (Xu et al., 2016). In the atmosphere, NH_3 can neutralize with H_2SO_4 and HNO_3 to produce ammonium sulfate and ammonium nitrate (Lanniello et al., 2010). These aerosols are the main components of $PM_{2.5}$ with accounting for 20%-60% of the $PM_{2.5}$ concentrations (Shen et al., 2014; Tao et al., 2012). So, the concentration of gaseous NH_3 in the atmosphere is affected not only by emissions, but also by the amount of acid gases in the atmosphere. In order to accurately assess NH_3 emission changes in China by inversion method described in Sect. 2.7,

acidic gases and their precursors (NOx and SO_2) were first corrected in this study.

Based on the linear correction method of Martin et al. (2003, 2006), NOx and SO_2 emissions were corrected using the data from the Environmental Air quality monitoring Network of China Monitoring Station. The distribution of air quality monitoring stations is shown in Figure 4-3. The time resolution is the monthly average, and the time is from 2013 to 2016.
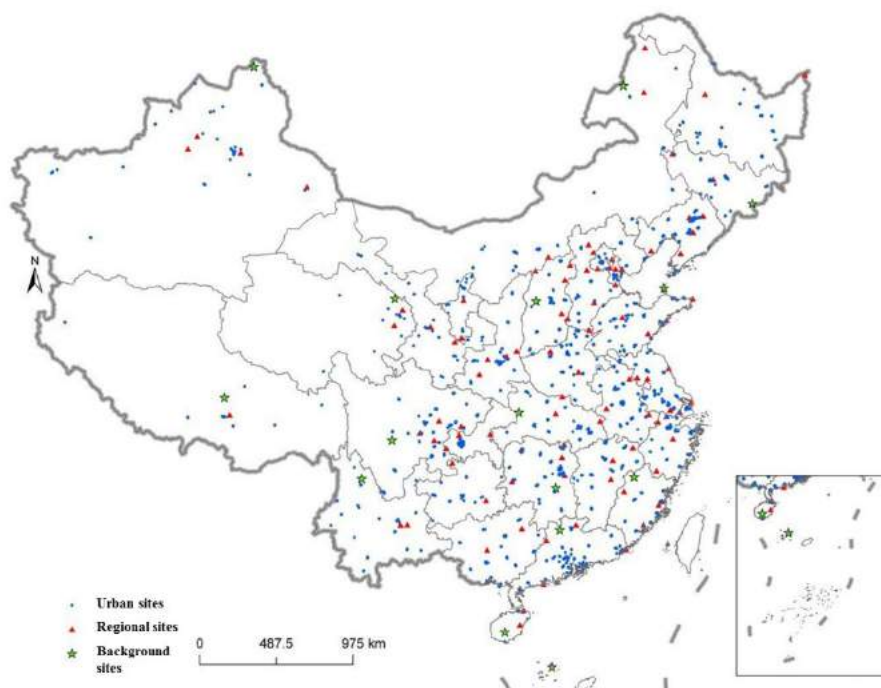

Figure 4-3. Spatial distribution of stations for air quality sites in China.

4.2.1 Validation the NOx emissions

Based on the MEIC inventory, NO_2 concentrations were simulated from 2013 to 2016. The comparison between the simulated and observed monthly average NO_2 concentrations was shown in Figure 4-4 in typical cities (Beijing, Tangshan, Tianjin, and Shijiazhuang). The results indicate that the simulated NO_2 based on MEIC are basically consistent with the trend of the observed values, and both show obvious seasonal variation characteristics, with low summer and high winter. In terms of annual changes, both the observed and simulated NO_2 concentrations decreased year by year from 2013 to 2016, with a significant decreasing trend. The uncertainty of simulated NO_2 concentration in the four cities ranged from 8% to 45%.

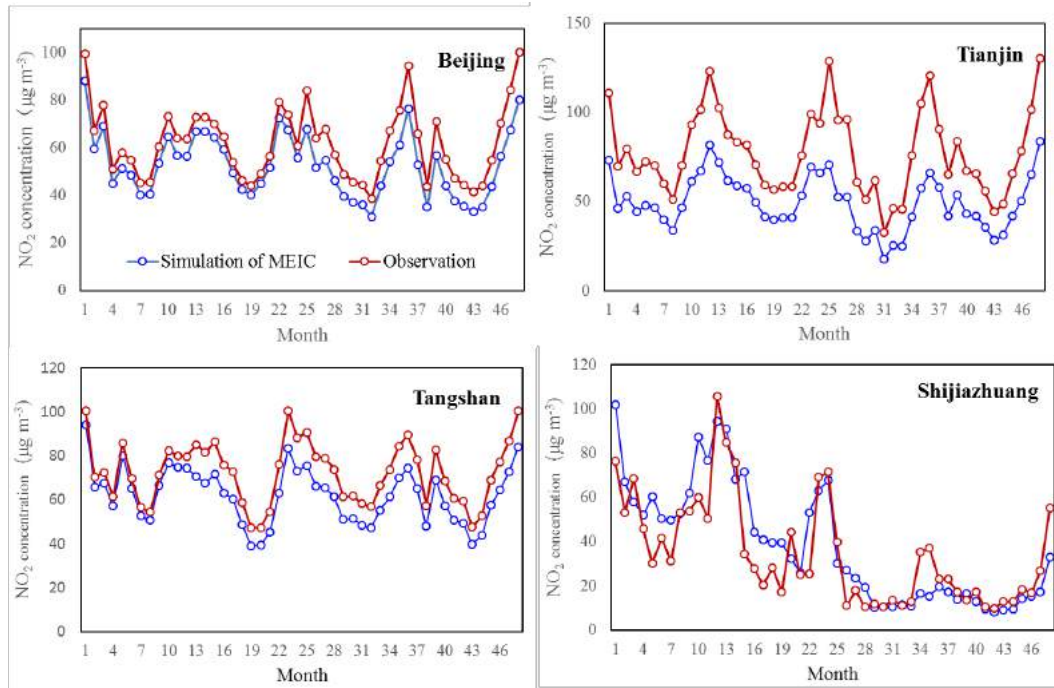Figure 4-4. The comparison between the simulated and observed monthly average NO$_2$ concentrations in typical cities.

The scatter validation result of the simulated NO$_2$ concentrations based on MEIC is shown in Figure 4-5. The simulated NO$_2$ concentrations are underestimated (43%) compared to the measured values, and the underestimation is mainly found in the values of less than 40 µg/m^3. In general, the simulated values are in good agreement with the observed values (R^2=0.55).
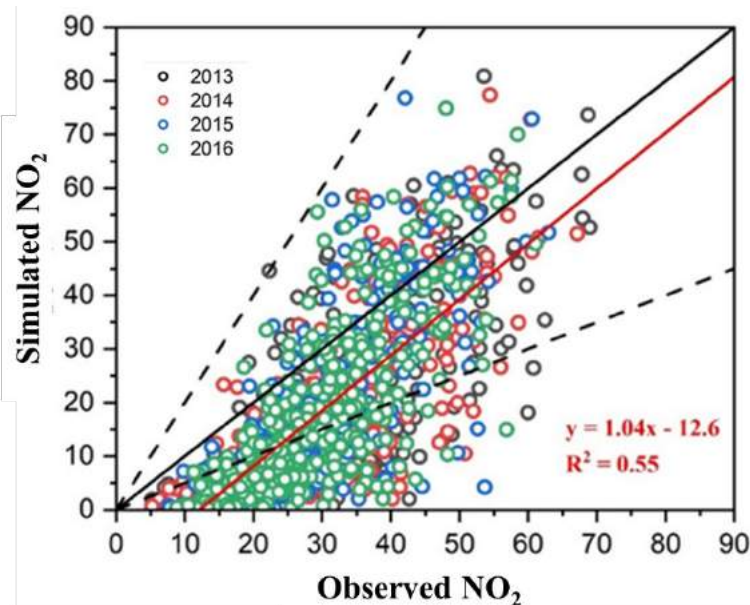

Figure 4-5. The scatter validation result of the simulated NO$_2$ concentrations based on MEIC from 2013 to 2016.

4.2.2 Improvement of SO$_2$ emissions

a. Correction coefficient matrix of SO$_2$

Due to the obvious spatial heterogeneity of ground monitoring sites (Figure 4-6), there are densely in eastern of China and rare in western of China. For reducing the error caused by the uneven distribution of site data, the mean of city was calculated, and then compared with the initial simulation results in order to obtain the correction coefficient matrix for spatial variability from 2013 to 2016. The results are shown in Figure 4-4. From The result shows that, except for a few cities, the SO_2 emission correction coefficient for most cities in China is less than 1, indicating the overestimation of the SO_2 emissions. The SO_2 correction coefficient of northeast China, Gansu Province and cities in southern China exceeds 4, indicating that the SO_2 emissions in these cities are underestimated.
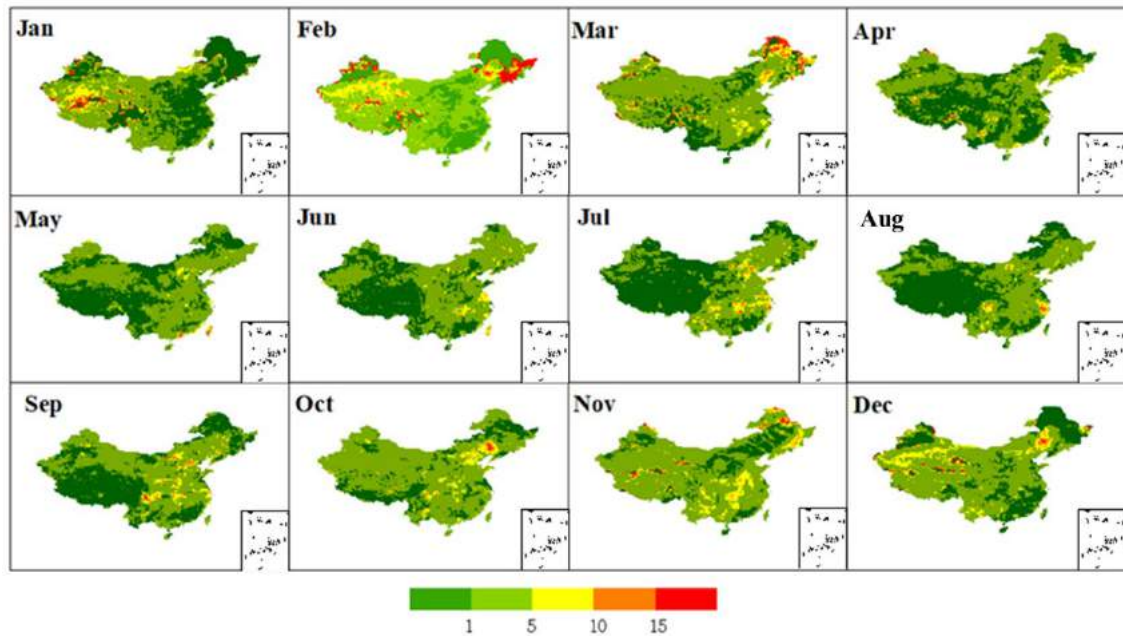

Figure 4-6. Monthly correction coefficient matrix of SO_2 based on initial simulation and observation.

b. Validation of the result

Based on the above space correction factors, the 2013–2016 emissions inventories were corrected and developed using the Inverse model. Figure4-7 shows the observed SO_2 concentrations in Chinese cities and the spatial distribution of the annual averages of simulated SO_2 concentrations before and after the inventories were corrected. According to the figures, the North China Plain, the Fenhe-Weihe River Plain, Northeast China, Xinjiang and Inner Mongolia are among the regions which mainly posted high observed concentrations of SO_2; the concentrations decreased year by year from 2013 to 2016 with a notable downward trend. It can be seen from the pre-correction EI simulations that the spatial distribution of high SO_2 concentrations throughout China was similar to the observations, yet the concentrations were higher than the observations and did not change greatly year by year. The simulated spatial distribution of SO_2 concentrations in the post-correction EIs was roughly consistent with the observations, and the concentrations declined obviously year by year; but the SO_2 concentrations in Qinghai were overestimated to a degree, possibly owing to the comparatively smaller amount of observation data. On the whole, the post-correction SO_2 concentrations featured good temporal-spatial coherence with the observations.
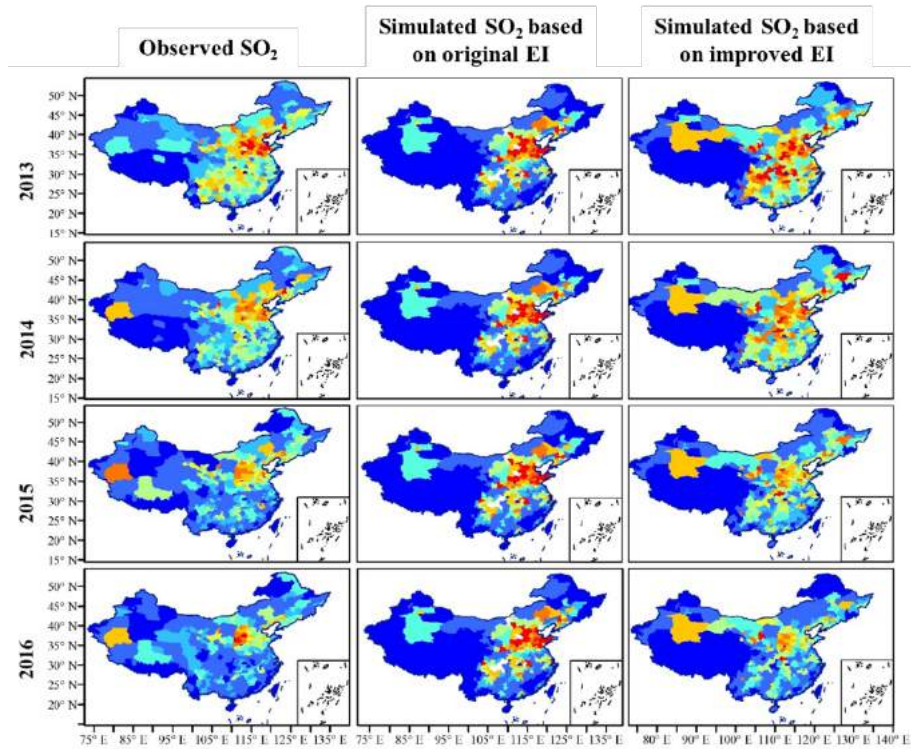
Figure 4-7. Spatial distribution of SO$_2$ measured concentration and simulated concentration before and after inventory correction in China from 2013 to 2016.

It is found from a comparison between the simulated and the observed monthly average concentrations of SO$_2$ in typical cities such as Beijing, Tangshan, Tianjin and Shijiazhuang during 2013–2016 (Figure 4-8) that modified simulated results were roughly consistent with corresponding observations and both showed significant seasonal variations (low in summer and high in winter). In terms of annual changes, both the observed and the simulated concentrations of SO$_2$ were on a striking decline from 2013 through to 2016. With respect to absolute concentrations, the simulated SO$_2$ concentrations in the four cities were overestimated by 6%–44%.
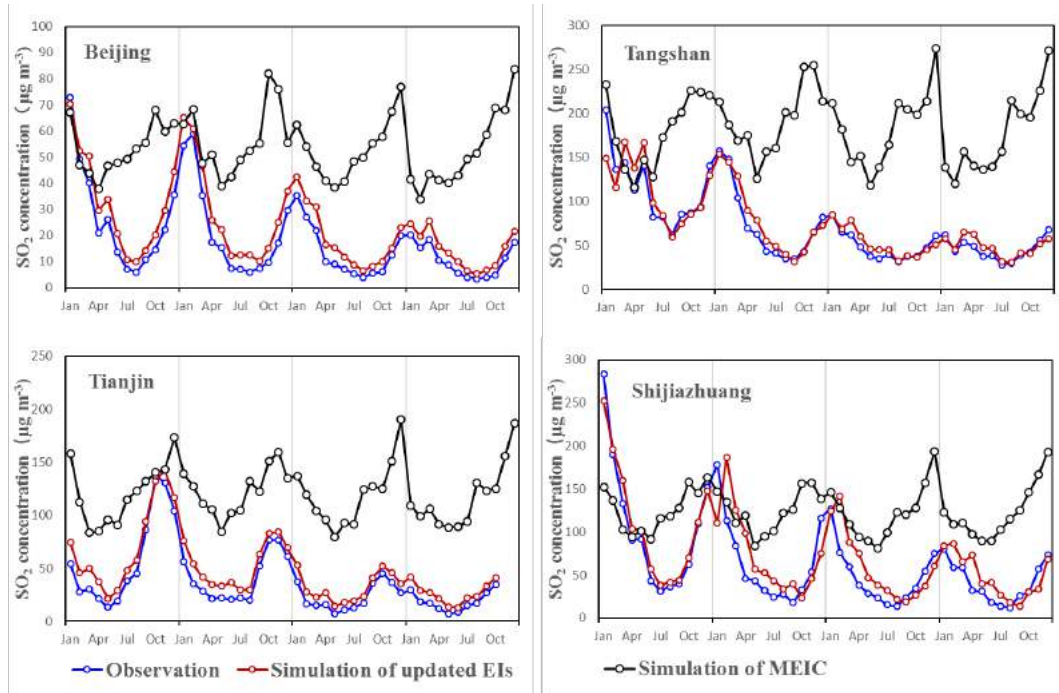
Figure 4-8. Comparison of simulation and observation of monthly average concentration by original and improved SO₂ inventory in typical cities in during 2013-2016.

The SO$_2$ EIs after correction were made much more precise, judging from the scatter plot of simulations vs observations (Figure 4-9). The annual average concentrations of SO$_2$ simulated in the original EIs were notably overestimated, while the simulated and observed concentrations had a low correlation to each other. The annual average concentrations of SO$_2$ simulated in the corrected EIs were of the same order of magnitude as the observations, and the correlation coefficient between the two reached 0.6, marking an obvious improvement and the simulations roughly in line with the observations.

Therefore, both spatial distribution and time variation justify the consistency between the post-correction SO$_2$ emissions and the actual results. On this basis, the NH$_3$ emission can be improved as the next step.
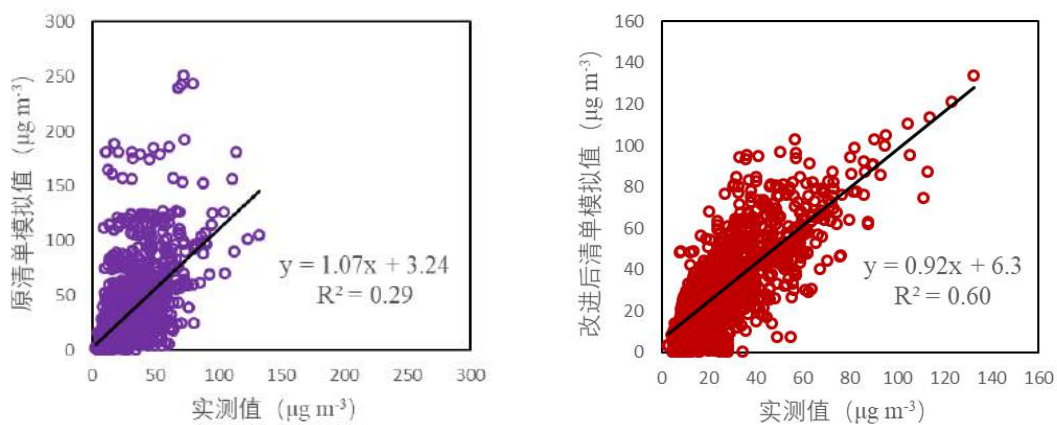

Figure 4-9. Verification of SO₂ simulated concentration between original inventory (left) and corrected inventory (right).

4.2.3 Correction of the monthly profiles of NH₃ emissions

Based on the relationship between monthly and annual concentrations observed by the satellites, a correction factors matrix for the 2013–2016 NH_3 emissions inventories reflecting the monthly changes was constructed. See Figure 4-10 for the results of 2014. Figure 4-8 shows the monthly profiles of NH_3 columns in China, which have obvious temporal and spatial variations. In summer months (June–August) it have the maximum percentage of NH_3 columns throughout a year, i.e. more than 10 percent in most parts of China and even over 20 percent in North China and Northeast China. However, NH_3 columns in each of all the other months contributed less than 10 percent to the annual total. Where, NH_3 columns in North China in autumn and winter made up for less than five percent in the annual total.

As discussed above, the concentration of atmospheric NH_3 is affected not only by NH_3 emissions but also by the concentration of acid gases. Considering the work above, SO_2 emission has been improved and the NOx emission is reasonable. In this step, the main reason for the uncertainty of simulated NH_3 concentrations is the NH_3 emissions. In this step, we assume that the different in observed data is the same as the difference in emissions. So the monthly value of NH_3 emission in MEIC was reassignment according to the correction factors matrix based on observed data.
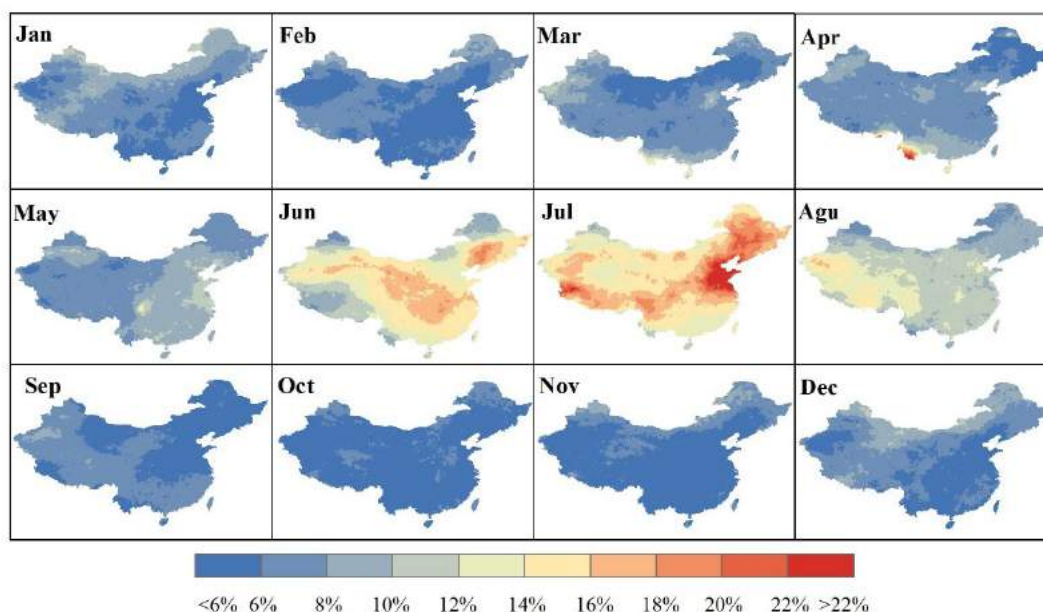

Figure 4-10. Monthly correction coefficient matrix of NH_3 emission inventory based on initial simulation and observation in 2014.

4.2.4 Validation of the NH₃ simulations

See Figure 4-11 for the validation results of model-simulated monthly NH_3 concentrations during 2013-2015 and Figure 4-12 for the validation parameters. After the EIs were corrected, the simulated NH_3 concentrations of most stations fell within the range of deviations, but those of a few stations were significantly overestimated or underestimated. For example, the simulated concentrations of QZ and WW stations were significantly underestimated, even beyond the range of deviations, while the simulations of LSD, CD and DL stations were overestimated to varying degrees.

Compared with the simulations of the original emissions inventories (Figure 4-11), in spite of the differences in the simulated and observed results in a few areas at certain time intervals, the overall results were satisfying. Most stations reported the average relative deviation of simulations at a range of -37 percent to 57 percent and the average relative error at a range of 46 percent to 73 percent. Only a very few stations were outside the two ranges.
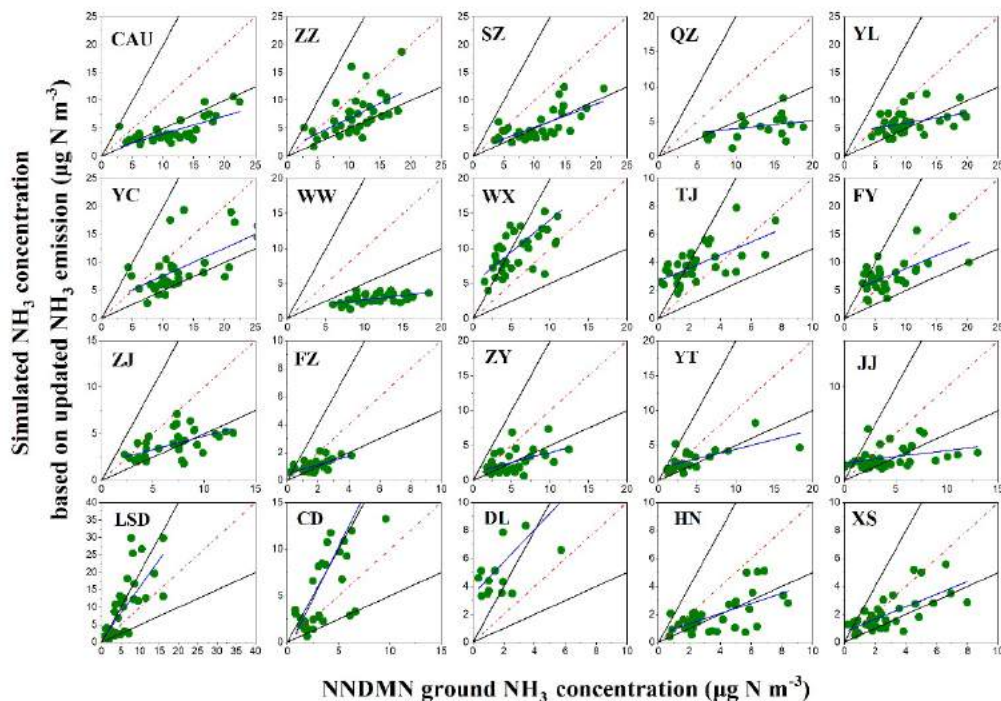

Figure 4-11. Comparison of simulated NH$_3$ concentration by corrected emission inventory with NNDMN station observed concentration.

Table 4-1. Parameter table of simulation concentration verification.

	Numbers	Intercept	Slope	r	p Value
CAU	35	0.81	0.32	0.72	<0.01
ZZ	36	1.48	0.53	0.58	<0.01
SZ	35	1.08	0.41	0.69	<0.01
QZ	35	2.81	0.12	0.34	<0.01
YL	35	4.13	0.19	0.39	<0.01
YC	35	2.62	0.50	0.61	<0.01
WW	35	1.48	0.12	0.53	<0.01
WX	36	4.97	0.91	0.61	<0.01
TJ	36	2.67	0.47	0.64	<0.01
FY	35	4.32	0.46	0.63	<0.01
ZJ	36	1.88	0.29	0.58	<0.01
FZ	36	0.51	0.31	0.63	<0.01
ZY	36	1.11	0.29	0.49	<0.01
YT	24	1.73	0.27	0.67	<0.01
JJ	35	1.87	0.14	0.36	<0.01
LSD	36	0.65	1.53	0.72	<0.01

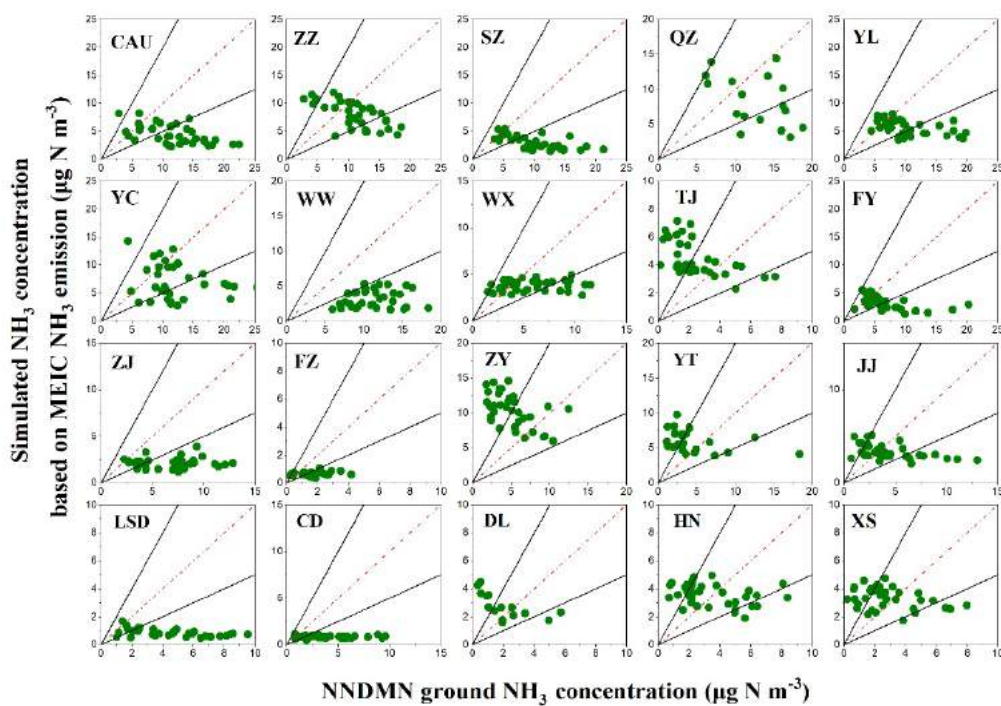| CD | 36 | -0.88 | 2.23 | 0.71 | <0.01 |
DL	15	3.42	1.16	0.64	<0.01
HN	36	0.61	0.36	0.63	<0.01
XS	36	0.75	0.45	0.68	<0.01

Figure 4-12. Comparison of simulated NH_3 concentration by original emission inventory with NNDMN station observed concentration.

4.3 Emission characteristics of NH_3 gases in China during 2013–2016
4.3.1 Comparison between original and corrected emissions inventories

When this study was conducted, emission data of MEIC were available only every two years. Therefore, emissions in 2014 and 2016 were compared in this study.

The inversion method of this study update NH_3 emission in monthly basis. See Figure 4-13 for the spatial changes in total monthly emissions before and after the correction. From the perspective of monthly variation, pre-correction NH_3 emissions did not show significant seasonal variation, with the exception of a minor increase in the North China Plain region during May–August only; but the post-correction NH_3 emissions varied significantly month by month, notably high in spring and summer and low in autumn and winter. Specifically, total NH_3 emissions in the eastern China regions including Northeast China (No.①), North China (No.②), the Fenhe-Weihe River Plain area (No.③), the Yangtze River Delta (No.④), the middle areas of the Yangtze River (No.⑤), Chengdu and Chongqing (No.⑥) and the Pearl River Delta (No.⑦) in June and July were significantly higher (above 7.5 kg N ha^{-1}) than the figures in the other months. The results showed that the monthly variation characteristics of NH_3 emission inventory were more obvious after correction, which was consistent with the actual emission factors (such as agricultural fertilization, soil ammonia release caused by temperature rise, etc.).
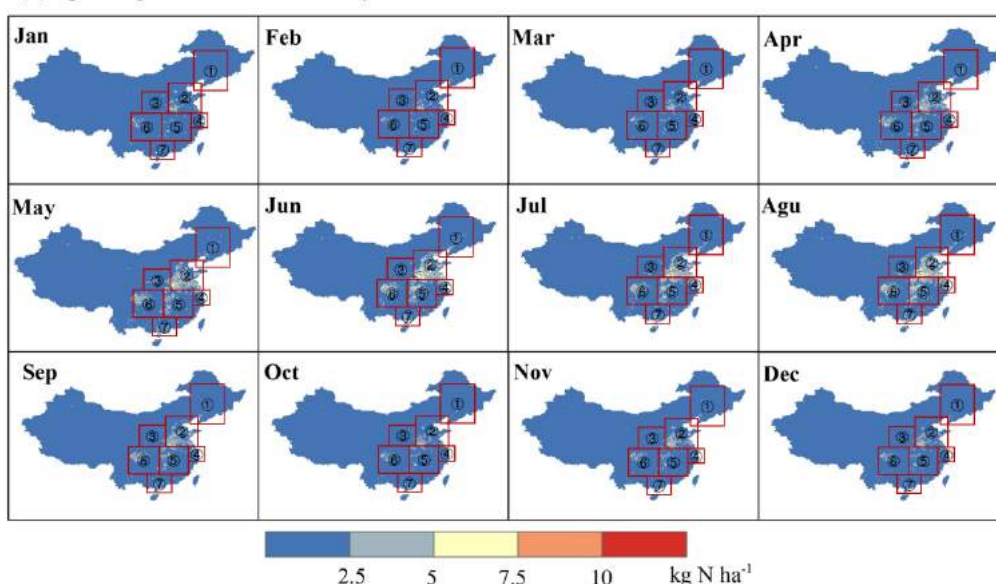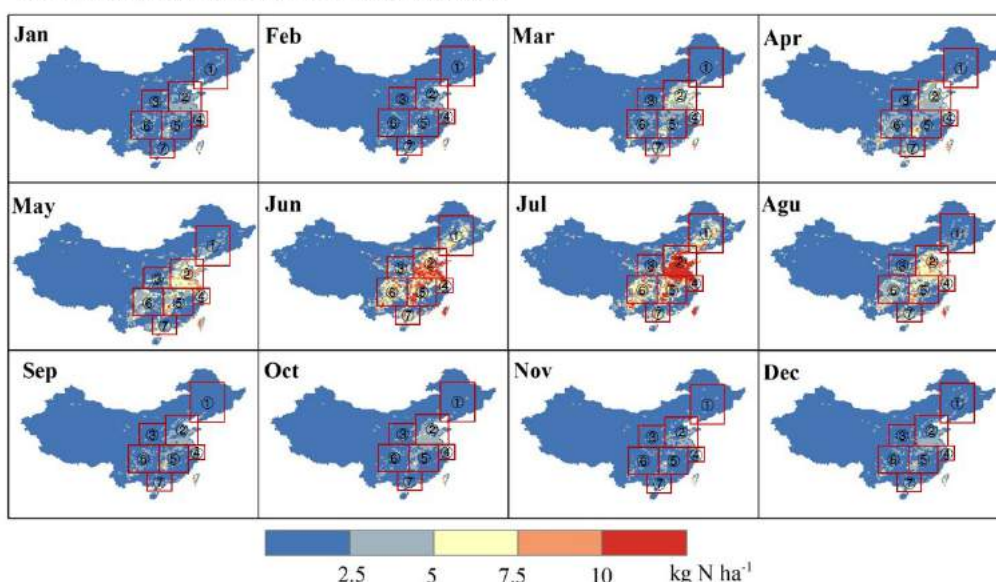
Figure 4-13. Comparison spatial distribution of original and corrected NH3 emission inventory averaged in 2014 and 2016.

Figure 4-14 clearly indicates that the monthly variation of NH$_3$ emissions in the MEIC is much smaller than those in the corrected EIs which shows significant seasonal variation, i.e. high in summer and low in winter; NH$_3$ emissions in summer in the corrected EIs were approximately 2.5 times of those in the original EIs. The analysis of observations shows notable seasonal variations in the concentrations of NH$_3$ in the air, hitting highs in summer and falling to lows in autumn and winter. The seasonal variation of NH$_3$ concentration is consistent with that of the improved NH$_3$ emissions although the seasonality of NH$_3$ concentration is determined not only by emissions, but also combined effects of emissions, meteorological conditions and chemical transformations in the air.
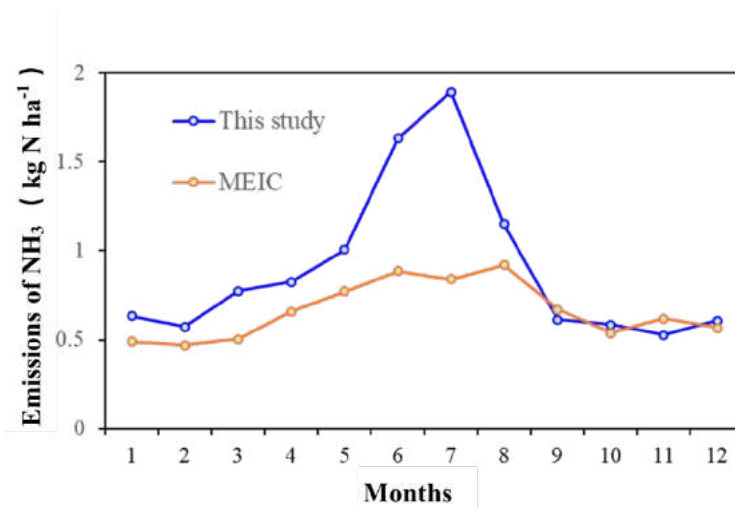
Figure 4-14. Comparison of monthly variation of NH₃ emissions between the MEIC inventor and the corrected one in this study.

4.3.2 Characteristics of temporal changes in NH₃ gas emissions in China during 2013–2016

This section analyzes the temporal-spatial changes in the emissions of nitrogen-containing gases in China during 2013–2016 based on the corrected NH₃ emissions inventories. The corrected NH₃ emissions in China showed almost stable trend from 2013 (about 9.6 million tons) to 2016 (about 10.2 million tons) (Figure 4-15). Compared to the emission amount of MEIC, the corrected emissions were decreased by 580 thousand tons in 2014 but were increased by 100 thousand tons or so in 2016 by inversion method of this study. Generally speaking, emissions corrected by inversion model are basically in line with those in the bottom-up emission inventory MEIC.
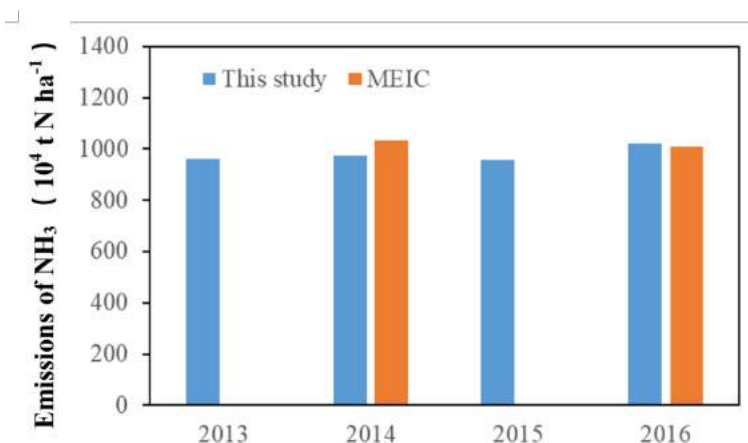
Figure 4-15. Annual characteristics of NH₃ emission in China from 2013 to 2016.

Regarding monthly variations (Figure 4-16), monthly NH₃ emissions from 2013 to 2014 were characterized by significant seasonal variations, with highs taking place in summer (up to 1-1.5 million tons) and lows appearing in autumn and winter (basically at 0.5 million tons), and general features of the seasonality were almost the same. The updated emissions inventories showed more significant changes in monthly variation than the MEIC, with the high emission figures in spring and summer (6-56 percent larger) and the low emission figures in autumn and

winter (1-40 percent lower). According to the features of monthly variations, the amounts of NH₃ emissions in China is stable. The reason may be that there are no efficient control measures to reduce NH₃ emissions in China.
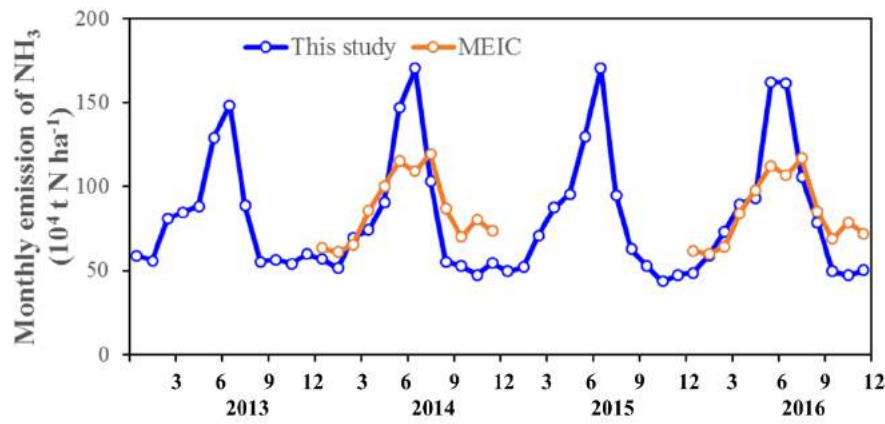
Figure 4-16. Monthly characteristics of NH₃ emission in China from 2013 to 2016.

4.3.2 Characteristics of spatial changes in NH₃ gas emissions in China during 2013–2016

From the perspective of spatial changes in China's NH₃ emissions during 2013–2016 (Figure 4-17), the country's NH₃ emissions in these years were roughly consistent by spatial distribution. The high emissions, which exceeded 50 kg ha^{-1} yr^{-1}, occurred in the North China Plain, the Yangtze River Delta, the Pearl River Delta, Chengdu and Chongqing regions with the densely populated and farmlands. The following is the northeastern and northwestern city clusters with value of 10-30 kg ha^{-1} yr^{-1}. And the lowest NH₃ emissions (less than 10 kg ha^{-1} yr^{-1}) appeared in the central and western regions in China with sparsely populated.
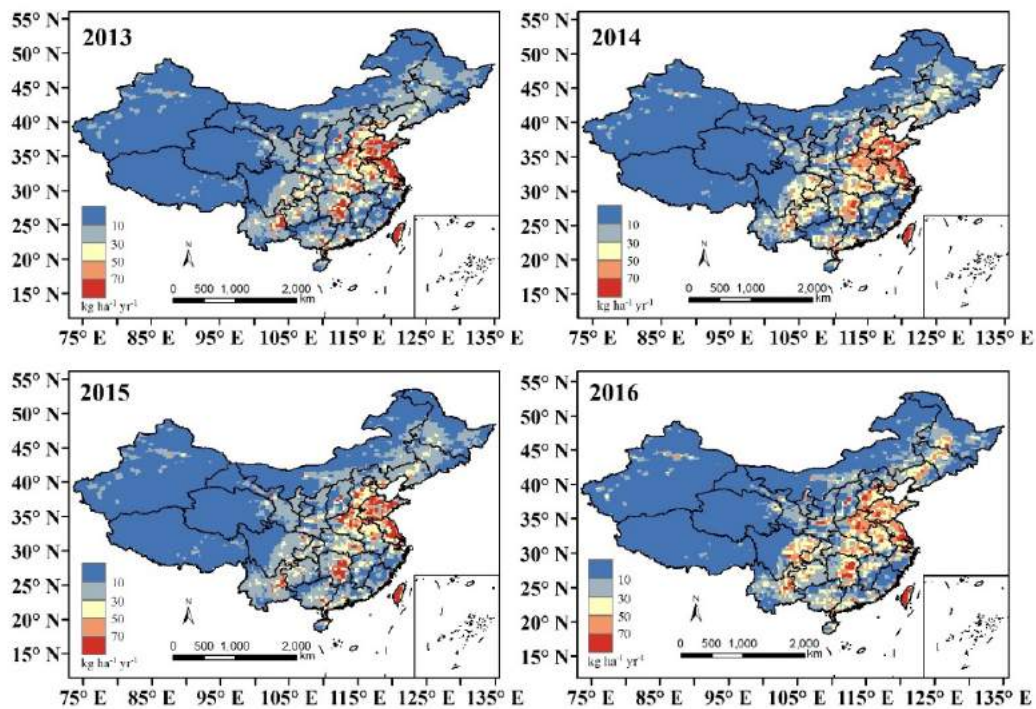

Figure 4-17. Spatial characteristics of NH₃ emission in China from 2013 to 2016.

5. Conclusions

Focusing on the Chinese mainland, the paper firstly assesses the reliability of observed temporal-spatial distribution of NH_3 column concentrations nationwide and the relevant trends using satellites over long time series. Then the national emission inventories of NH_3 were improved with the inverse model on the basis of the satellite observations. The paper draws the following conclusions mainly:

First, the reliability of the trend of temporal and spatial changes in NH_3 concentrations observed by satellites is examined through the NH_3 mass concentrations observed on the ground. According to the results, the NH_3 column concentrations observed by satellites feature good temporal-spatial coherence with the ground-based observations of mass concentration, and thus, are considered to reflect the temporal-spatial change characteristics of NH_3 concentrations in the air in China over long time series. In China, NH_3 concentrations in the air are characterized by significant temporal-spatial changes. In terms of spatial distribution, high NH_3 column concentrations in the troposphere are mainly distributed in the most developed regions such as the North China Plain region, the Yangtze River Delta, the Pearl River Delta, Chengdu and Chongqing. It can be seen that intense human activity significantly increases NH_3 emission in the atmosphere. In terms of the annual variation, the concentrations of Tropospheric NH_3 column in China showed a notable increasing trend. From the perspective of seasonal changes, NH_3 column concentrations have the highest value in summer and the lowest in autumn or winter.

In this study, the NH_3 emissions inventories were improved using atmospheric chemical transport model, satellite observations, and inverse modeling methodology. Then, the updated EI accuracy is validated by the observations at ground stations. Gaseous NH_3 concentrations in the air are influenced not only by its emissions but also by the content of acid gases in the air. There are two steps to improve the NH_3 emission inventory in this study. Firstly, SO_2 emission was correction before correcting the NH_3 emissions inventory. The bottom-up SO_2 emission inventories were updated by inverse modeling approach using the ground-based observation data. The simulated SO_2 concentrations using the corrected SO_2 emissions were consistent with the temporal and spatial variations of the ground-based monitoring data and thus, it is considered that SO_2 emissions were well corrected for the inverse modeling of NH_3 emissions. Then, monthly NH_3 emissions were improved using inverse modeling based on satellite observation. The simulated results of NH_3 concentrations using the updated emissions were validated using the monthly averages of data observed at NNDMN Station, and the result shows the corrected emissions inventories were improved in terms of spatial distribution and time variation characteristics. In terms of spatial distribution, according to the corrected emissions, NH_3 emissions were mainly seen in densely-populated areas such as the North China Plain, the Yangtze River Delta, the Pearl River Delta, Chengdu and Chongqing, with the emissions per unit area exceeding 300 kg ha^{-1} yr^{-1}. As for annual changes, China showed almost stable trend in NH_3 emissions from 2013 to 2016, and nationwide NH_3 emissions came in at about 10 million tons in each of these years.

The research, which attempted to improve the emissions inventories of atmospheric NH_3 based on the satellite data and with the method of Martin et al. (2003, 2008), still has lots of limitations. This method assumes a linear relationship in the simulation grid (36 km × 36 km) when dealing with the relationship between emissions and concentrations. It does not take into

consideration the non-linear relationship between emissions and concentrations in the surrounding grids, nor the observation data and model errors. In fact, the influence of transportation between grids cannot be ignored. In addition, there are large uncertainties in satellite observations and systematic errors in the models. Furthermore, similar to influences of SO_2 and NO_x emissions on NH_3 concentrations, emissions of NH_3 also affects concentrations of SO_2 and NO_x. These complex system of the chemical transformation in the atmosphere were not considered in the methodology of this study. Recently, the advancement of data assimilation technology has come with the introduction of Kalman filtering and four-dimensional assimilation technology into improving the air pollutant emissions inventories. These two methods give sufficient consideration to the influence of atmospheric transportation and incorporate observation and simulation errors to correct pollutant emissions data. Further efforts should be made to improve air pollutant emissions rapidly and in real time with better technologies and methods and in overall consideration of transportation and errors.

References

Boersma, K.F., D.J. Jacob, H.J. Eskes, R.W. Pinder, J. Wang, 2008. Intercomparison of SCIAMACHY and OMI tropospheric NO_2 columns: Observing the diurnal evolution of chemistry and emissions from space. Journal of Geophysical Research: Atmospheres (1984–2012), 113(D16).

Cheng, M., H. Jiang, Z. Guo, X. Zhang, X. Lu, 2013. Estimating NO_2 dry deposition using satellite data in eastern China. International Journal of Remote Sensing, 34(7): 2548-2565.

Cheng, M.M., Zhi, G.R., Tang, W., Liu, S.J., Dang, H.Y., Guo, Z., Du, J.H., Du, X.H., Zhang, W.Q., Zhang, Y.J., 2017. Air pollutant emission from the underestimated households' coal consumption source in China. Science of The Total Environment, 580, 641-650.

Clarisse, L., Clerbaux, C., Dentener, F., Hurtmans, D., Coheur, P.-F., 2009. Global ammonia distribution derived from infrared satellite observations. Nat. Geosci., 2(7), 479-483.

Fowler, D., Steadman, C.E., Stevenson, D., Coyle, M. Rees,R.M., Skiba, U. M., Sutton, M.A., Cape, J.N., Dore, A.J.. Vieno, M., Simpson, D., Zaehle, S., Stocker, B.D., Rinaldi, M., Facchini, M.C., Flechard, C.R., Nenitz, E., Twigg, M., Erisman, J.W., Butterbach-Bahl, K., Galloway, J.N., 2015. Effects of global change during the 21st century on the nitrogen cycle. Atmospheric Chemistry and Phisics 15, 13849-13893.

Galloway, J. N. and E. B. Cowling, 2002. Reactive nitrogen and the world: 200 years of change, AMBIO: A Journal of the Human Environment, 31. 64-71.

Galloway, J. N., A. R. Townsend, J. W. Erisman, M. Bekunda, Z. Cai, J. R. Freney, L. A. Martinelli, S. P. Seitzinger, and M. A. Sutton, 2008. Transformation of the nitrogen cycle: recent trends, questions, and potential solutions, Science, 320. 889-892.

Holland, E. A., B. H. Braswell, J. Sulzman, and J.-F. Lamarque., 2005. Nitrogen deposition onto the United States and Western Europe: synthesis of observations and models, Ecological applications, 15. 38-57.

Holland, E. A., F. J. Dentener, B. H. Braswell, and J. M. Sulzman, 1999. "Contemporary and pre-industrial global reactive nitrogen budgets," in New Perspectives on Nitrogen Cycling in the Temperate and Tropical Americas, ed: Springer, pp. 7-43.

Huang, X., Song, Y., Li, M.M. Li, J.F., Huo, Q., Cai, X.H., Zhu, T., Hu, M., Zhang, H. S., 2012.

A high-resolution ammonia emission inventory in China. Global Biogeochemical Cycles, 26, GB1030, doi:10.1029/2011GB004161..

Huang, Z., S. Wang, J. Zheng, Z. Yuan, S. Ye, and D. Kang., 2015. Modeling inorganic nitrogen deposition in Guangdong province, China, Atmospheric Environment, 109. 147-160.

Kang, Y., Liu, M., Song, Y., Huang, X., Yao, H., Cai, X., Zhang, H., Kang, L., Liu, X., Yan, X., He, H., Zhang, Q., Shao, M., Zhu, T., 2016. High-resolution ammonia emissions inventories in China from 1980 to 2012. Atmospheric Chemistry and Physics, 16(4): p. 2043-2058.

Kurokawa, J. I., Y. I. Uno, and T. Ohara, 2009. Adjoint Inverse Modeling Of NOx Emissions Over Eastern China Using Satellite Observations Of NO_2 Vertical Column Densities, Atmospheric Environment, 43. 1878-1887.

Kurokawa, J., Ohara, T., Morikawa, T., Hanayama, S., Greet, J. -M., Fukui, T., Kawashima, K., Akimoto, H., 2013. Emissions of air pollutants and greenhouse gases over Asian regions during 2000-2008: Regional Emission inventory in Asia (REAS) version 2. Atmos Chem Phys Dis. Atmospheric Chemistry & Physics, 13(4): 10049-10123.

Lamarque, J. F., J. Kiehl, G. Brasseur, T. Butler, P. Cameron-Smith, W. Collins, W. Collins, C. Granier, D. Hauglustaine, and P. Hess, 2005. Assessing future nitrogen deposition and carbon cycle feedback using a multimodel approach: Analysis of nitrogen deposition, Journal of Geophysical Research: Atmospheres (1984–2012), 110.

Lamsal, L., R. Martin, A. Van Donkelaar, M. Steinbacher, E. Celarier, E. Bucsela, E. Dunlea, and J. Pinto, 2008. Ground‑level nitrogen dioxide concentrations inferred from the satellite‑borne Ozone Monitoring Instrument, Journal of Geophysical Research: Atmospheres (1984–2012), 113.

Li, M., Zhang, Q., Kurokawa, J.-I., Woo, J.-H., He, K., Lu, Z., Ohara, T., Song, Y., Streets, D. G., Carmichael, G. R., Cheng, Y., Hong, C., Huo, H., Jiang, X., Kang, S., Liu, F., Su, H., and Zheng, B., 2017. MIX: a mosaic Asian anthropogenic emission inventory under the international collaboration framework of the MICS-Asia and HTAP. Atmospheric Chemistry and Physics, 17(2): p. 935-963.

Li, M., Zhang, Q., Streets, D. G., He, K. B., Cheng, Y. F., Emmons, L. K., Huo, H., Kang, S. C., Lu, Z., Shao, M., Su, H., Yu, X., Zhang, Y., 2013. Mapping Asian anthropogenic emissions of non-methane volatile organic compounds to multiple chemical mechanisms. Atmospheric Chemistry & Physics Discussions, 13(11): 32649-32701.

Liang, T., Y. Tong, W. Lin, L. Qiao, X. Liu, S. Bai, and X. Yang., 2014. Spatial-temporal variability of dry and wet deposition of atmospheric nitrogen in different ecological regions of Shaanxi, Acta Ecologica Sinica, 34. 738-745.

Lin, J. T., 2012. Satellite constraint for emissions of nitrogen oxides from anthropogenic, lightning and soil sources over East China on a high-resolution grid, Atmospheric Chemistry & Physics, 12. 2881-2898.

Liu, F., Zhang, Q., Tong, D., Zheng, B., Li, M., Huo, H., He, K. B., 2015. High-resolution inventory of technologies, activities, and emissions of coal-fired power plants in China from 1990 to 2010. Atmospheric Chemistry & Physics, 15: 18787-18837.

Liu, L., Zhang, X., Wong, A. Y. H., Xu, W., Liu, X., Li, Y., Mi, H., Lu, X., Zhao, L., Wang, Z., Wu, X., and Wei, J., 2019. Estimating global surface ammonia concentrations inferred from

satellite retrievals, Atmos. Chem. Phys., 19, 12051–12066, https://doi.org/10.5194/acp-19-12051-2019.

Liu, L., Zhang, X., Xu, W., Liu, X., Li, Y., Lu, X., Zhang, Y., Zhang, W., 2017a. Temporal characteristics of atmospheric ammonia and nitrogen dioxide over China based on emission data, satellite observations and atmospheric transport modeling since 1980. Atmos. Chem. Phys., 17(15), 9365-9378.

Liu, L., Zhang, X., Xu, W., Liu, X., Lu, X., Wang, S., Zhang, W., Zhao, L., 2017b. Ground ammonia concentrations over China derived from satellite and atmospheric transport modeling. Remote. Sens., 9(5), 467.

Liu, X., D. Lei, J. Mo, E. Du, J. Shen, X. Lu, Z. Ying, X. Zhou, C. He, and F. Zhang., 2011. Nitrogen deposition and its ecological impact in China: An overview, Environmental Pollution, 159. 2251-64.

Liu, X., X. Ju, Y. Zhang, C. He, J. Kopsch, and Z. Fusuo., 2006. Nitrogen deposition in agroecosystems in the Beijing area, Agriculture, ecosystems & environment, 113. 370-377.

Liu, X.J., Zhang, Y., Han, W.X., Tang, A., Shen, J.L., Cui, Z.L., Vitousek, P., Erisman, J.W., Goulding, K., Christie, P., Fangmeier, A., Zhang, F.S., 2013. Enhance nitrogen deposition over China. Nature, 494,459-462.

Lu, C. and H. Tian, 2014. Half-century nitrogen deposition increase across China: A gridded time-series data set for regional environmental assessments, Atmospheric Environment, 97. 68–74.

Lü, C. and H. Tian., 2007. Spatial and temporal patterns of nitrogen deposition in China: synthesis of observational data, Journal of Geophysical Research: Atmospheres (1984–2012), 112.

Lü, C.Q., Tian, H.Q., 2007. Spatial and temporal patterns of nitrogen deposition in China: Synthesis of observational data. Journal of Geophysical Research: Atmosphere 112, D22S05.

Magill, A. H., J. D. Aber, G. M. Berntson, W. H. McDowell, K. J. Nadelhoffer, J. M. Melillo, and P. Steudler., 2000. Long-term nitrogen additions and nitrogen saturation in two temperate forests, Ecosystems, 3. 238-253.

Martin, R. V., C. E. Sioris, C. Kelly, T. B. Ryerson, T. H. Bertram, P. J. Wooldridge, R. C. Cohen, N. J. Andy, S. Aaron, and F. M. Flocke., 2006. Evaluation of space-based constraints on global nitrogen oxide emissions with regional aircraft measurements over and downwind of eastern North America, Journal of Geophysical Research Atmospheres, 111. 3363-3375.

Martin, R. V., D. J. Jacob, K. Chance, T. P. Kurosu, P. I. Palmer, and M. J. Evans., 2003. Global inventory of nitrogen oxide emissions constrained by space‐based observations of NO_2 columns, Journal of Geophysical Research: Atmospheres (1984–2012), 108(D17).

Mo, J. M., Xue, J. H. and Fang, T. Y., 2004. Litter decomposition and its responses to simulated N deposition for the major plants of Dinghushan forest in subtropical China, Acta. Ecologica. Sinica., 24(7). 1413-1420.Shen, J., A. Tang, X. Liu, A. Fangmeier, K. Goulding, F. Zhang, 2009. High concentrations and dry deposition of reactive nitrogen species at two sites in the North China Plain. Environmental Pollution, 157(11): p. 3106-3113.

She W. Hu Huanyong: father of China's population geography. China Popul Today. 1998

Aug;15(4):20. PMID: 12294257.

Streets, D. G., T. Canty, G. R. Carmichael, B. D. Foy, R. R. Dickerson, B. N. Duncan, D. P. Edwards, J. A. Haynes, D. K. Henze, and M. R. Houyoux., 2013. Emissions estimation from satellite retrievals: A review of current capability, Atmospheric Environment, 77. 1011-1042.

Streets, D.G., Zhang, Q., Wang, L., He, K., Hao, J., Wu, Y., Tang, Y., Carmichael, G. R., 2006. Revisiting China's CO emissions after the Transport and Chemical Evolution over the Pacific (TRACE-P) mission: Synthesis of inventories, atmospheric modeling, and observations. Journal of Geophysical Research Atmospheres, 111(D14).

Sutton, M.A., Reis, S., Riddick, S.N. Dragosits, U., Nemitz,E., Theobald, M.R., Tang, Y.S., Braban, C.F., Vieno, M., Dore, A.J., Mitchell, R.F., Wanless, S., Daunt, F., Flower, D., Blackall, T.D., Milford, C., Flechard, C.R., Louber, B., Massad, R., Cellier, P., Personne, E., Coheur, P. F., Clarisse, L., Van Damme, M., Ngadi, Y., Clerbaux, C., Skjoth, C.A., Geels, C., Hertel, O., Kruit, R.J.W., Pinder, R. W., Bash, J.O., Walker, J.T., Simpson, D., Horvath, L., Misselbrook, T.H., Bleeker, A., Dentener, F., De Vries, W., 2013, Towards aclimate-dependent paradigm of ammonia emission and deposition. Philosophical Transactions of the Royal Society B-Biological Scences 368,20130166.Van Damme M, Clarisse L, Whitburn S, Hadji-Lazaro J, Hurtmans D, Clerbaux C, Coheur P-F. 2018. Industrial and agricultural ammonia point sources exposed. Nature 564, 99-103. Van Damme M, Whitburn S, Clarisse L, Clerbaux C, Hurtmans D, Coheur PF., 2017. Version 2 of the IASI NH_3 neural network retrieval algorithm: near-real-time and reanalysed datasets. Atmos. Meas. Tech., 10(12), 4905-4914.

Van Damme, M., Clarisse, L., Dammers, E., Liu, X., Nowak, J., Clerbaux, C., Flechard, C., Galy-Lacaux, C., Xu, W., Neuman, J., 2015. Towards validation of ammonia (NH_3) measurements from the IASI satellite. Atmos. Meas. Tech., 8(3), 1575-1591.

Van Damme, M., Clarisse, L., Hurtmans, D. R., Ngadi, Y., Clerbaux, C., Dolman, A. J., Erisman, J. W., Coheur, P. -F., Heald, Colette L., 2014. Global distributions, time series and error characterization of atmospheric ammonia (NH_3) from IASI satellite observations. Atmospheric Chemistry and Physics, 14(6): p. 2905-2922.

Whitburn, S., Van Damme, M., Clarisse, L., Bauduin, S., Heald, C. L., Hadji-Lazaro, J., Hurtmans, D., Zondlo, M. A., Clerbaux, C., and Coheur, P.-F., 2016. A flexible and robust neural network IASI NH_3 retrieval algorithm. J. Geophys. Res.-Atmos., 121, 6581-6599.

Xu, W., Goulding, K. W. T., 2015. Quantifying atmospheric nitrogen deposition through a nationwide monitoring network across China. Atmospheric Chemistry and Physics, 15(21): p. 12345-12360.

Xu, W., Liu, L., Cheng, M., Zhao, Y., Zhang, L., Pan, Y., Zhang, X., Gu, B., Li, Y., Zhang, X., Shen, J., Lu, L., Luo, X., Zhao, Y., Feng, Z., Collett Jr., J. L., Zhang, F., and Liu, X., 2018. Spatial-temporal patterns of inorganic nitrogen air concentrations and deposition in eastern China. Atmospheric Chemistry and Physics Discussions, 18, 10931–10954, https://doi.org/10.5194/acp-18-10931-2018.

Zhang, Q., D. G. Streets, K. He, Y. Wang, A. Richter, J. P. Burrows, I. Uno, C. J. Jang, D. Chen, and Z. Yao., 2007. NOx emission trends for China, 1995-2004: The view from the ground and the view from space. Journal of Geophysical Research Atmospheres, 112(D22):

449-456.

Zhao, C. and Y. Wang, 2009. Assimilated inversion of NOx emissions over east Asia using OMI NO_2 column measurements, Geophysical Research Letters, 36. 150-164.

Zyrichidou, I., M. E. Koukouli, D. Balis, K. Markakis, A. Poupkou, E. Katragkou, I. Kioutsioukis, D. Melas, K. F. Boersma, and M. V. Roozendael., 2014. Identification of surface NOx emission sources on a regional scale using OMI NO_2, Atmospheric Environment, 101. 82-93.